

Article

Transient Wave Propagation in Functionally Graded Viscoelastic Structures

Sergey Pshenichnov ¹, Radan Ivanov ² and Maria Datcheva ^{3,*}¹ Institute of Mechanics, Lomonosov Moscow State University, 119192 Moscow, Russia² National Institute of Geophysics, Geodesy and Geography, Bulgarian Academy of Sciences, 1113 Sofia, Bulgaria³ Institute of Mechanics, Bulgarian Academy of Sciences, 1113 Sofia, Bulgaria

* Correspondence: datcheva@imbm.bas.bg

Abstract: Transient wave processes in viscoelastic structures built from functionally graded material (FGM) still remain almost unexplored. In this article, the problem of the propagation of nonstationary longitudinal waves in an infinite viscoelastic layer of a FGM with plane-parallel boundaries is considered. The physical and mechanical parameters of the FGM depend continuously on the transverse coordinate, while the wave process propagates along the same coordinate. The viscoelastic properties of the material are taken into account employing the linear integral Boltzmann–Volterra relations. The viscoelastic layer of the FGM is replaced by a piecewise-homogeneous layer consisting of a large number of sub-layers (a package of homogeneous layers), thus approximating the continuous inhomogeneity of the FGM. A solution of a non-stationary dynamic problem for a piecewise-homogeneous layer is constructed and, using a specific example, the convergence of the results with an increase in the number of sub-layers in the approximating piecewise-homogeneous layer is shown. Furthermore, the problem of the propagation of nonstationary longitudinal waves in the cross section of an infinitely long viscoelastic hollow FGM cylinder, whose material properties continuously change along the radius, is also considered. The cylinder composed of the FGM is replaced by a piecewise-homogeneous one, consisting of a large number of coaxial layers, for which the solution of the non-stationary dynamic problem is constructed. For both the layer and the cylinder composed of a viscoelastic FGM, the results of calculating the characteristic parameters of the wave processes for the various initial data are presented. The influence of the viscosity and inhomogeneity of the material on the dynamic processes is demonstrated.

Keywords: functionally graded materials; wave processes; viscoelasticity; dynamics of layered bodies; inhomogeneous layer; inhomogeneous cylinder

MSC: 74D05

Citation: Pshenichnov, S.; Ivanov, R.; Datcheva, M. Transient Wave Propagation in Functionally Graded Viscoelastic Structures. *Mathematics* **2022**, *10*, 4505. <https://doi.org/10.3390/math10234505>

Academic Editors: Hovik Matevossian, Maria Korovina and Sergey Lurie

Received: 1 November 2022

Accepted: 21 November 2022

Published: 29 November 2022

Publisher's Note: MDPI stays neutral with regard to jurisdictional claims in published maps and institutional affiliations.



Copyright: © 2022 by the authors. Licensee MDPI, Basel, Switzerland. This article is an open access article distributed under the terms and conditions of the Creative Commons Attribution (CC BY) license (<https://creativecommons.org/licenses/by/4.0/>).

1. Introduction

Materials with spatial heterogeneity are widely used in various fields of modern industry and are the subject of research in many areas of science. This explains the growing interest in the study of functionally graded materials (FGM) with a continuous dependence of physical and mechanical properties on spatial coordinates and, in particular, in the study of wave processes in such materials.

Publications devoted to the study of the dynamic behavior of continuously inhomogeneous elastic solids using analytical and numerical–analytical methods first appeared several decades ago [1–5]. At that time, in the study of non-stationary wave processes in such solids, analytical methods using integral transforms of various types [1–3], and numerical–analytical methods were developed to solve problems of the propagation of harmonic elastic waves [4,5]. Modern advances in the field under consideration are detailed,

for example, in the review papers [6–8]. In addition, a review of studies of vibrations in thin-walled structural elements made of FGM is contained in [9,10].

Among the methods used to study wave processes in FGM, matrix methods of various types based on the reduction of the equations of dynamics to a system of first order differential equations are widespread. With their help, a number of studies of stationary wave processes in inhomogeneous elastic waveguides were carried out [11,12]. In [13,14], the dispersion of Lamb waves in elastic FG plates was studied using the power series method. The “orthogonal polynomial approach” [15,16] also finds wide application in dynamic problems for FGM. In addition, along with the conventional finite element method, the Semi-Analytical Finite Element Method (SAFE) has been used [17,18].

When studying harmonic oscillations, as well as harmonic waves in FG waveguides, a common approach is the approximation of the continuously inhomogeneous material such as the FGM, by a layered structure with continuity conditions at the interfaces between the layers. This approach is expressed in various modifications of the transfer matrix method, which was used to study stationary wave processes in elastic FG half-spaces, layers, and plates [19,20], as well as piezoelectroelastic FG films and cylinders [21,22].

The vibration behavior of FGMs also exhibits notable temperature and moisture dependence as demonstrated in [23]. This dependence has been studied regarding stationary wave propagation in FG porous sandwich plates [24] by a higher-order shear deformation theory (HSDT). This theory was applied to analyze the stationary wave propagation in porous plates resting on a viscoelastic foundation [25] and it was applied in conjunction with nonlocal elasticity theory to dynamics of FG nanoplates [26].

In recent years, progress has been made in the field of studying the problems of the diffraction of sound harmonic waves on solids with continuously inhomogeneous elastic [27] and thermoelastic [28] coatings using the spline collocation method in combination with analytical methods. The above-mentioned works [27,28] also contain a brief review of publications on this topic.

It is to be noted that the vast majority of publications on FGM dynamics are devoted to stationary wave processes (harmonic oscillations and waves), and mainly within the framework of linear elasticity, thermoelasticity, and piezoelectroelasticity. However, one should not ignore the fact that the study of non-stationary waves in FGM, which started in the last century [1–3], continues in the last decades and has its important place in research related to FGM dynamics [29–31].

It is also important to note that there are much fewer publications on the dynamics of viscoelastic FGM. Stationary waves have been studied within the framework of the Kelvin–Voigt viscoelastic model [32,33] and the Kelvin–Voigt fractional model [34]. Harmonic oscillations are considered using the standard viscoelastic body model in [35]. The listed works contain references to other publications on the dynamics of viscoelastic FGM, but their number is relatively small. Transient wave processes in viscoelastic structures from FGM, however, still remain practically unexplored. In the available literature, to the best of our knowledge, there are no publications on this topic (with a few exceptions, such as [36] and several other publications by the first author of the present work).

In this regard, the aim of the present work is to investigate the unsteady dynamics of some canonical solids (e.g., a layer and a hollow cylinder) consisting of viscoelastic FGM. It should be emphasized that the problem concerns transient wave processes. This implies the development of methods used in stationary dynamic problems leading to their application to non-stationary problems. The solid composed of a FGM is replaced by a piecewise-homogeneous body consisting of a large number of homogeneous components (e.g., layers), whereby at the component interfaces the displacement and stress vectors are considered continuous, and the physical and mechanical properties of the layers approximate the continuously varied material properties of the FGM. The advantage of this method is the ability to use the already constructed solutions of non-stationary dynamic problems for piecewise-homogeneous (layered) solids. However, its applicability in the study of transient wave processes, even for solids with smooth boundaries and continuity of the

external loads, is not obvious. This is because, on the one hand, with a sufficiently large number of homogeneous layers approximating the FGM, the properties of adjacent layers will differ little, but on the other hand, the contact interfaces of the layers will be a source of additional disturbances. Due to the difficulty of providing a rigorous mathematical justification of the proposed approach, in this paper we restrict ourselves to confirming its validity for specific examples by performing the appropriate calculations. It is to be noted that, in the study of transient wave processes in FGM solids, this approach was already successfully applied in the case of linear elasticity [37]. For viscoelastic FGMs, some results have been obtained in the framework of the linear Boltzmann–Volterra model with a two-parameter exponential kernel (i.e., for standard linear solids) [36].

In this paper, we present the results for singular viscoelastic kernels within the framework of the same Boltzmann–Volterra model. Furthermore, for a viscoelastic piecewise-homogeneous layer with parallel constituent homogeneous layers (homogeneous layer bundle), the solution of the unsteady dynamic problem is constructed in a form convenient for obtaining quantitative results. The nature of transient wave processes in a layer of viscoelastic FGM, as well as in a hollow cylinder of viscoelastic FGM, is studied for the selected material properties and constitutive functions.

The results of the present study can be used to a different extent to model the propagation of non-stationary disturbances in viscoelastic coatings on rigid substrates and in tubes produced, for example, by additive manufacturing, or in tubes produced by coiling. Furthermore, the results obtained here can be used to verify numerical algorithms and the performance of engineering software packages. Another useful and important outcome is that this study has confirmed the possibility of using the method to approximate the continuous inhomogeneity of FGM by a set of homogeneous layers, particularly in nonstationary dynamic elastic and viscoelastic problems.

2. Formulation of the Dynamics Problem for an Inhomogeneous Viscoelastic Layer

Let us consider the problem of the propagation of nonstationary longitudinal waves in a viscoelastic infinite layer of thickness L with parallel boundaries, whose material properties continuously depend on the transverse coordinate X . The viscoelastic properties will be taken into account within the framework of the linear Boltzmann–Volterra model.

The layer is initially at rest, one of its boundaries ($X = 0$) is fixed, and on the other ($X = L$), starting at time $t = 0$, a uniformly distributed normal load $P(t)$ is applied. Thus, the wave process propagates in the direction of the material properties variation. Let us introduce the following dimensionless quantities:

$$x = X/L, \tau = t/t_0, u(x, \tau) = u_X(X, t)/L,$$

$$\sigma_1(x, \tau) = \sigma_X(X, t)/[2G_0(x)], P_0 f(\tau) = P(t)/[2G_0(1)],$$

$$\gamma_s(x, \tau) = t_0 T_s(X, t), \gamma_v(x, \tau) = t_0 T_v(X, t),$$

where $u_X(X, t)$, $\sigma_X(X, t)$ are the displacement and the stress, $t_0 = L/c(1)$, $c(x) = \sqrt{2w(x)G_0(x)/\rho(x)}$ is the velocity of the longitudinal elastic wave; $w(x) = [1 - \nu_0(x)]/[1 - 2\nu_0(x)]$, $G_0(x)$, $\nu_0(x)$ are the instantaneous values of the shear modulus and Poisson’s ratio, $T_s(X, t)$, $T_v(X, t)$ are the shear and bulk relaxation kernels, $\rho(x)$ denotes density, P_0 is a dimensionless constant. In Figure 1a are shown the loading conditions.



Figure 1. Loading of the layer’s cross section. (a) FG layer; (b) piecewise-homogeneous layer.

The mathematical formulation of the problem in dimensionless form includes the equation of dynamics:

$$\frac{\partial \sigma_1(x, \tau)}{\partial x} + \left\{ \frac{d}{dx} \ln \left[\frac{G_0(x)}{G_0(1)} \right] \right\} \sigma_1(x, \tau) = w(x) \frac{c^2(1)}{c^2(x)} \frac{\partial^2 u(x, \tau)}{\partial \tau^2}, \quad 0 \leq x \leq 1, \quad (1)$$

the boundary conditions:

$$u(0, \tau) = 0, \quad \sigma_1(1, \tau) = -P_0 f(\tau), \quad \tau > 0 \quad (2)$$

and the initial conditions:

$$u(x, 0) = 0, \quad \frac{\partial}{\partial \tau} u(x, 0) = 0, \quad 0 \leq x \leq 1, \quad (3)$$

where

$$\begin{aligned} \sigma_1(x, \tau) &= w(x) (1 - \hat{d}_1) \frac{\partial u(x, \tau)}{\partial x}, \quad \hat{d}_1 \xi(\tau) = \int_0^\tau d_1(x, \tau - \chi) \xi(\chi) d\chi, \\ d_1(x, \tau) &= \frac{1}{3[1-\nu_0(x)]} \{ [1 + \nu_0(x)] \gamma_v(x, \tau) + 2 [1 - 2\nu_0(x)] \gamma_s(x, \tau) \} \end{aligned} \quad (4)$$

Consider a similar problem with the same boundary conditions for a piecewise-homogeneous layer of the same thickness L , consisting of N homogeneous layers: $X_{n-1} \leq X \leq X_n$, ($n = 1, 2, \dots, N$; $X_0 = 0$; $X_N = L$; $N \gg 1$) with continuity conditions for displacement and stresses vectors at the contact $X = X_m$ between the layers ($m = 1, 2, \dots, N - 1$). Let us designate by $G_0^{(n)}, \nu_0^{(n)}, \rho_n, c_n, T_v^{(n)}(t), T_s^{(n)}(t)$ the instantaneous values of the shear modulus and Poisson’s ratio, as well as the density, the velocity of the longitudinal elastic waves, the kernels of the bulk and shear relaxation for the n th layer, and by $u_X^{(n)}(X, t), \sigma_X^{(n)}(X, t)$ the displacement and the stress in the n th layer. We approximate the functions characterizing the properties of the material of the original functionally graded layer using the relations ($n = 1, 2, \dots, N$):

$$\begin{aligned} G_0^{(n)} &= G_0(x_n), \quad \nu_0^{(n)} = \nu_0(x_n), \quad \rho_n = \rho(x_n), \\ \gamma_v^{(n)}(\tau) &= \gamma_v(x_n, \tau), \quad \gamma_s^{(n)}(\tau) = \gamma_s(x_n, \tau). \end{aligned}$$

Here $x_n = X_n/L, \tau = t/t_0, t_0 = L/c(1) = L/c_N$ as $c_n = c(x_n)$. In this way, $\gamma_v^{(n)}(\tau) = t_0 T_v^{(n)}(t), \gamma_s^{(n)}(\tau) = t_0 T_s^{(n)}(t), P_0 f(\tau) = P(t)/(2G_0^{(N)})$. In addition, we introduce the dimensionless quantities $u^{(n)}(x, \tau) = u_X^{(n)}(X, t)/L, \sigma_1^{(n)}(x, \tau) = \sigma_X^{(n)}(X, t)/(2G_0^{(n)}), \alpha_n = c_N/c_n, w_n = w(x_n) = (1 - \nu_0^{(n)})/(1 - 2\nu_0^{(n)})$. The problem setup is shown schematically in Figure 1b. Note that the thickness and number of layers has to be chosen in the way to obtain reasonably good approximation of the FGM properties.

The formulation of the problem in dimensionless form for a piecewise-homogeneous layer includes the equations:

$$(1 - \hat{d}_1^{(n)}) \frac{\partial^2}{\partial x^2} u^{(n)}(x, \tau) - \alpha_n^2 \frac{\partial^2}{\partial \tau^2} u^{(n)}(x, \tau) = 0, \quad x_{n-1} \leq x \leq x_n, \quad x_0 = 0, \quad x_N = 1, \quad (5)$$

with boundary conditions:

$$u^{(1)}(0, \tau) = 0, \quad \sigma_1^{(N)}(1, \tau) = -P_0 f(\tau) \quad (6)$$

initial conditions:

$$u^{(n)}(x, 0) = 0, \quad \frac{\partial}{\partial \tau} u^{(n)}(x, 0) = 0 \quad (7)$$

and the conditions at the interfaces between layers:

$$u^{(m)}(x_m, \tau) = u^{(m+1)}(x_m, \tau), \quad G_0^{(m)} \sigma_1^{(m)}(x_m, \tau) = G_0^{(m+1)} \sigma_1^{(m+1)}(x_m, \tau) \quad (8)$$

herewith,

$$\begin{aligned} \sigma_1^{(n)}(x, \tau) &= w_n(1 - d_1^{(n)}) \frac{\partial u^{(n)}(x, \tau)}{\partial x}, \quad d_1^{(n)} \zeta(\tau) = \int_0^\tau d_1^{(n)}(\tau - \chi) \zeta(\chi) d\chi, \\ d_1^{(n)}(\tau) &= \frac{1}{3(1-\nu_0^{(n)})} [(1 + \nu_0^{(n)}) \gamma_v^{(n)}(\tau) + 2(1 - 2\nu_0^{(n)}) \gamma_s^{(n)}(\tau)] \end{aligned} \tag{9}$$

We assume that all hereditary kernels satisfy the condition of limited creep.

3. Solution Method for a Piecewise-Homogeneous Layer

The integral Laplace transform is applied to Equations (5), (6), (8), (9), denoting the images of $u^{(n)}(x, \tau)$, $\sigma_1^{(n)}(x, \tau)$, $f(\tau)$, $d_1^{(n)}(\tau)$ as $U^{(n)}(x, s)$, $S_1^{(n)}(x, s)$, $F(s)$, $D_1^{(n)}(s)$ (s —complex variable), respectively. The solution in the images domain reads:

$$\begin{aligned} U^{(n)}(x, s) &= \frac{F_0 F(s) p_n}{\beta_N Z(s)} [\zeta_1^{(n)} \text{sh}(y_n) + \zeta_2^{(n)} \text{ch}(y_n)], \quad y_n = x \alpha_n \beta_n, \quad n = 1, 2, \dots, N, \\ S_1^{(n)}(x, s) &= \frac{F_0 F(s)}{\beta_N Z(s)} p_n q_n \alpha_n \beta_n [\zeta_1^{(n)} \text{ch}(y_n) + \zeta_2^{(n)} \text{sh}(y_n)] \end{aligned} \tag{10}$$

where

$$\begin{aligned} \beta_n &= s / \sqrt{1 - D_1^{(n)}(s)}, \quad q_n = w_n(1 - D_1^{(n)}), \quad n = 1, 2, \dots, N, \\ Z(s) &= q_N [\zeta_1^{(N)} \text{ch}(\beta_N) + \zeta_2^{(N)} \text{sh}(\beta_N)] \\ p_N &\equiv 1, \quad p_m = -p_{m+1} q_{m+1}, \quad (m \leq N - 1) \\ \begin{pmatrix} \zeta_1^{(1)} \\ \zeta_2^{(1)} \end{pmatrix} &= \begin{pmatrix} 1 \\ 0 \end{pmatrix}, \quad \begin{pmatrix} \zeta_1^{(m+1)} \\ \zeta_2^{(m+1)} \end{pmatrix} = \begin{pmatrix} \eta_{11}^{(m)} & \eta_{12}^{(m)} \\ \eta_{21}^{(m)} & \eta_{22}^{(m)} \end{pmatrix} \begin{pmatrix} \zeta_1^{(m)} \\ \zeta_2^{(m)} \end{pmatrix}, \quad m = 1, 2, \dots, N - 1 \end{aligned}$$

The expressions for the matrix elements $\eta_{ij}^{(m)}$ are in the form:

$$\begin{aligned} \eta_{11}^{(m)} &= q_{m+1} \text{sh}(b_1^{(m)}) \text{sh}(b_2^{(m)}) - q_m \delta^{(m)} \text{ch}(b_1^{(m)}) \text{ch}(b_2^{(m)}), \\ \eta_{12}^{(m)} &= q_{m+1} \text{ch}(b_1^{(m)}) \text{sh}(b_2^{(m)}) - q_m \delta^{(m)} \text{sh}(b_1^{(m)}) \text{ch}(b_2^{(m)}), \\ \eta_{21}^{(m)} &= q_m \delta^{(m)} \text{ch}(b_1^{(m)}) \text{sh}(b_2^{(m)}) - q_{m+1} \text{sh}(b_1^{(m)}) \text{ch}(b_2^{(m)}), \\ \eta_{22}^{(m)} &= q_m \delta^{(m)} \text{sh}(b_1^{(m)}) \text{sh}(b_2^{(m)}) - q_{m+1} \text{ch}(b_1^{(m)}) \text{ch}(b_2^{(m)}), \end{aligned}$$

where

$$\delta^{(m)} = \frac{G_0^{(m)} \alpha_m \beta_m}{G_0^{(m+1)} \alpha_{m+1} \beta_{m+1}}, \quad b_1^{(m)} = x_m \alpha_m \beta_m, \quad b_2^{(m)} = x_m \alpha_{m+1} \beta_{m+1}, \quad m = 1, 2, \dots, N - 1.$$

Let us consider the case where $f(\tau) = h(\tau)$ is the Heaviside function and $F(s) = 1/s$. Let the relaxation kernels $\gamma_v^{(n)}(\tau)$, $\gamma_s^{(n)}(\tau)$ belong to the class of functions expressed as:

$$\sum_{k=1}^K a_k \exp(-b_k \tau), \quad \sum_{k=1}^K a_k / b_k < 1, \quad a_k > 0, \quad b_k > 0 \quad (k = 1, 2, \dots, K), \tag{11}$$

The constants a_k , b_k and K are specific for each particular kernel. The images of the relaxation kernels have no branch points in the complex plane. Then the solutions $U^{(n)}$, $S_1^{(n)}$ in images (10) also have no branch points, in spite of the fact that the functions β_n have branch points. This follows from the general theorem [38] and can also be seen by expanding the hyperbolic functions included in the expressions (10) into power series. Note that the roots of the equations $1 - D_1^{(n)} = 0$ are the limit points of the set of poles of the functions $U^{(n)}$, $S_1^{(n)}$. We will consider the case when all these roots are real and simple.

Then, after asymptotic studies of images $U^{(n)}, S_1^{(n)}$ in the vicinity of the infinitely distant point, as well as in the vicinity of the finite limit points of the set of their poles, the originals $u^{(n)}, \sigma_1^{(n)}$ are represented in the form of a series of residues at the corresponding poles:

$$\begin{aligned}
 u^{(n)}(x, \tau) &= u_0^{(n)}(x) + \sum_k \operatorname{Res}_{\substack{s=s_k \\ s \neq 0}} [U^{(n)}(x, s)e^{s\tau}], \quad u_0^{(n)}(x) = \operatorname{Res}_{s=0} [U^{(n)}(x, s)e^{s\tau}], \\
 \sigma_1^{(n)}(x, \tau) &= -\frac{G_0^{(N)}}{G_0^{(n)}} P_0 + \sum_k \operatorname{Res}_{\substack{s=s_k \\ s \neq 0}} [S_1^{(n)}(x, s)e^{s\tau}]
 \end{aligned}
 \tag{12}$$

where

$$\begin{aligned}
 u_0^{(n)}(x) &= -P_0 \frac{p_n^{(0)}}{\zeta_1^{(0)(N)} q_N^{(0)}} [\zeta_1^{(0)(n)} x + \zeta_2^{(0)(n)}], \quad x_{n-1} \leq x \leq x_n, \quad x_0 = 0, \quad x_N = 1, \\
 q_n^{(0)} &= w_n [1 - D^{(n)}(0)], \quad n = 1, 2, \dots, N \\
 p_N^{(0)} &\equiv 1, \quad p_m^{(0)} = -p_{m+1}^{(0)} q_{m+1}^{(0)}, \quad m = 1, 2, \dots, N - 1 \\
 \begin{pmatrix} \zeta_1^{(0)(1)} \\ \zeta_2^{(0)(1)} \end{pmatrix} &= \begin{pmatrix} 1 \\ 0 \end{pmatrix}, \quad \begin{pmatrix} \zeta_1^{(0)(m+1)} \\ \zeta_2^{(0)(m+1)} \end{pmatrix} = \begin{pmatrix} -\frac{G_0^{(m)}}{G_0^{(m+1)}} q_m^{(0)} & 0 \\ (\frac{G_0^{(m)}}{G_0^{(m+1)}} q_m^{(0)} - q_{m+1}^{(0)}) x_m & -q_{m+1}^{(0)} \end{pmatrix} \begin{pmatrix} \zeta_1^{(0)(m)} \\ \zeta_2^{(0)(m)} \end{pmatrix}.
 \end{aligned}$$

Finding the poles of the functions $U^{(n)}, S_1^{(n)}$, i.e., zeros of the function $Z(s)$, can be conducted in the same way as described in [39] for the case of the similar problem of a layered viscoelastic cylinder.

For relaxation kernels of a general form, the solution in originals is given in the form:

$$\begin{aligned}
 u^{(n)}(x, \tau) &= \frac{1}{2} u_0^{(n)}(x) + \frac{1}{\pi} \int_0^\infty \operatorname{Re}[U^{(n)}(x, i\omega)e^{i\omega \tau}] d\omega \\
 \sigma_1^{(n)}(x, \tau) &= -\frac{G_0^{(N)}}{2G_0^{(n)}} P_0 + \frac{1}{\pi} \int_0^\infty \operatorname{Re}[S_1^{(n)}(x, i\omega)e^{i\omega \tau}] d\omega, \quad n = 1, 2, \dots, N
 \end{aligned}
 \tag{13}$$

It is important to emphasize that if all homogeneous layers are linear elastic, then formulas (13) cannot be used, since in this case the imaginary axis contains the poles of the functions $U^{(n)}, S_1^{(n)}$. For other external load functions, the solution is built on the basis of expressions (12) or (13) using the well-known convolution operation (Duhamel integral).

4. Numerical Results for a FG Viscoelastic Layer

Using the numerical implementation of the constructed solution for a piecewise-homogeneous layer, studies of wave processes with various input data were carried out. When approximating the continuously varied material properties of a functionally graded layer by a certain number of homogeneous layers, the convergence of the results with an increase in the number of these layers is verified under the condition $\lim_{\tau \rightarrow 0} f(\tau) = 0$. Figure 2 illustrates such convergence in the case when the external load is a “smoothed step function” $f(\tau) = (1 - e^{-50\tau})h(\tau)$ with the following values of the material parameters and dependence on x :

$$\nu_0 \equiv 0.3, \quad \rho(x)/\rho(0) \equiv 1, \quad G_0(x)/G_0(0) = e^{-2x}, \quad \gamma_v \equiv 0, \quad \gamma_s = \gamma_s(\tau) = 0.1e^{-0.3\tau} \tau^{-0.2}.$$

Note that for the chosen $f(\tau)$ function, $P(t)$ tends to $2G_0(1)P_0$ when $t \rightarrow \infty$. The curves in Figure 2 show at point $x = 0$ for the different number of sub-layers: $N = 20, 40, 80$, (curves 1, 2 and 3, respectively) the variation with the time of the relative stress κ defined as

$$\kappa(x, \tau) = G_0(x)\sigma_1(x, \tau) / [G_0(1)P_0] = \sigma_X(X, t) / [2G_0(1)P_0]$$

For each N , the layers' thickness is taken to be equal to $1/N$. With the further increase in N ($N > 80$), there is no significant change in the results. Note, the negative stresses are compressive ($P_0 > 0$). Similar convergence is observed for the displacement and the velocity.

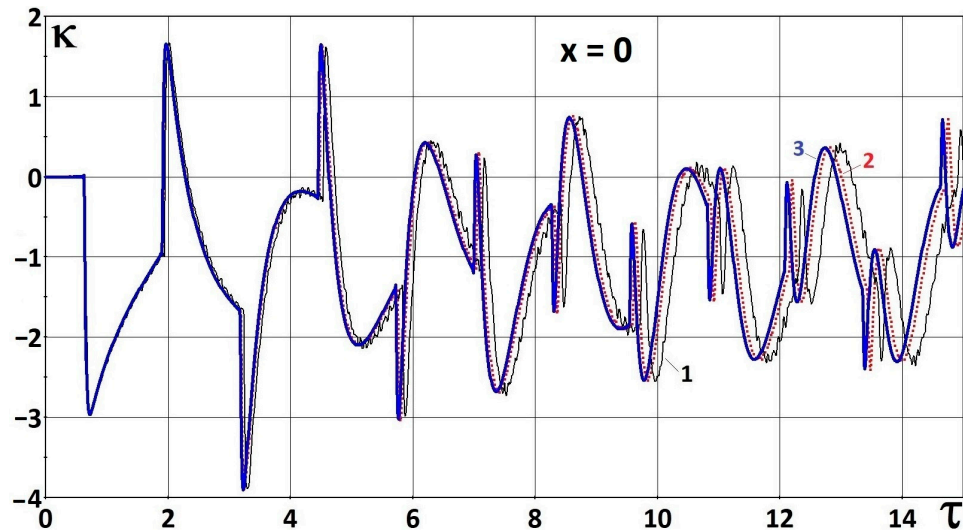


Figure 2. Time history of the relative stress at $x = 0$ with different number of sub-layers: $N = 20, 40, 80$ (curves 1, 2 and 3, respectively).

Along with the demonstrated convergence of the computational process with increasing the number of layers of the approximate representation of the FGM properties, the reliability of the estimated parameters of the unsteady wave process in structures made of FGM was also confirmed by additional verification. First, for the layer composed of FGM, at a given value of x , it is analytically determined without using the proposed method of multilayer approximation the dimensionless arrival time $\tau_f^{FGM}(x)$ to the point x of the first wave front counted from the boundary where the load is applied. Representing the velocity of the longitudinal elastic wave as $c(x) = c(1)\varphi(x)$, where $\varphi(x)$ is dimensionless, we get $\tau_f^{FGM}(x) = \int_x^1 \frac{d\xi}{\varphi(\xi)}$. Then τ_f^{FGM} was compared with $\tau_f^{(N)}(x)$, obtained by formulas (12) or (13) for the corresponding piecewise homogeneous layer of N homogeneous sublayers. For various types of FGM continuous inhomogeneity and for all selected values of x , the value of $\tau_f^{(N)}(x)$ has been found to tend to $\tau_f^{FGM}(x)$ with increasing N . For example, for the above considered FGM layer $\tau_f^{FGM}(0) = 0.632$ (rounding to the third decimal place). Approximating the FGM of the layer by multiple homogeneous layers (corresponding to Figure 2) we get $\tau_f^{(20)}(0) = 0.648$, $\tau_f^{(40)}(0) = 0.640$, $\tau_f^{(80)}(0) = 0.636$. Moreover, $\tau_f^{FGM}(0.5) = 0.393$ while $\tau_f^{(20)}(0.5) = 0.403$, $\tau_f^{(40)}(0.5) = 0.398$, $\tau_f^{(80)}(0.5) = 0.396$. Validation was similarly performed by comparing the arrival times at the selected points on the first wave fronts reflected from the boundaries and the comparison shows the same accuracy. In addition, it may be noted that the results obtained using formulas (12) or (13) for the special case $N = 1$ (homogeneous viscoelastic layer) were compared in our previous work [40] with the results obtained by finite element modeling in the ABAQUS environment, and a very good agreement between these results was demonstrated in [40].

The results presented below for the various inhomogeneous materials were obtained with the number of the homogeneous layers discretizing the FGM layer equal to 80. Here again $f(\tau) = (1 - e^{-50\tau})h(\tau)$. In the problem under consideration, among the various

characteristics of the wave process, of greatest interest is the variation in time of the relative stress at the fixed boundary $\kappa(0, \tau)$. In Figure 3 $\kappa(0, \tau)$ is shown by curve 1 calculated for the following material parameters and constitutive functions:

$$\nu_0 \equiv 0.3, \rho(x)/\rho(0) = G_0(x)/G_0(0) = e^{-2x}, \gamma_v \equiv 0, \gamma_s = \gamma_s(\tau) = 0.1e^{-0.3\tau}\tau^{-0.2}.$$

Thus, the density and the instantaneous shear modulus decrease exponentially in the direction from the fixed boundary to the boundary where the load is applied, but the velocity of the longitudinal elastic waves does not depend on x . Curve 2 was obtained with the same input data, but for the case of a linear elastic material ($\gamma_v \equiv \gamma_s \equiv 0$). Curve 3 is obtained for the case of the homogeneous viscoelastic material for which $\rho(x)/\rho(0) = G_0(x)/G_0(0) \equiv 1$.

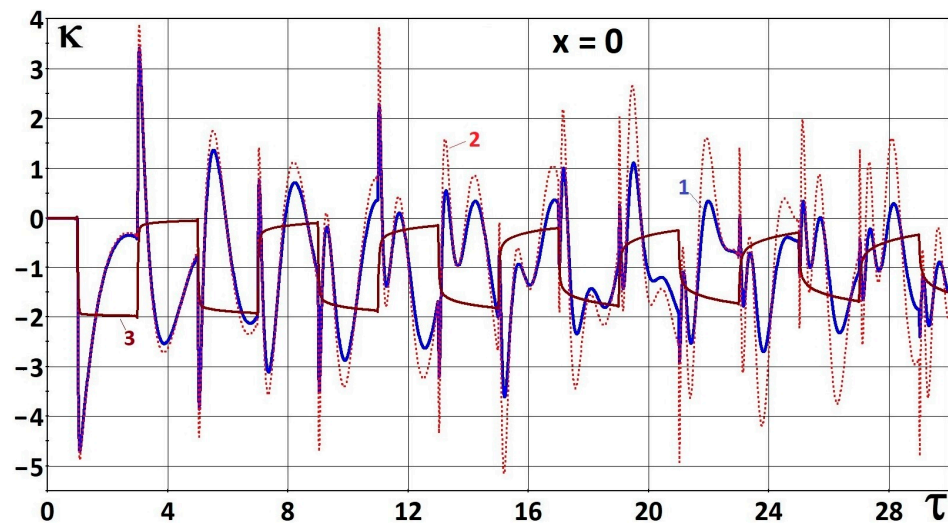


Figure 3. Relative stress–time history at $x = 0$ for viscoelastic FGM—curve 1, for elastic FGM—curve 2, for homogeneous viscoelastic material—curve 3.

It can be seen from Figures 2 and 3 that heterogeneity in the properties of the materials of the type considered here leads at certain times to the occurrence at the fixed boundary of the significant tensile stresses.

Figure 4 shows the same curve 1 of Figure 3 compared with curve 2, which is obtained when the density and instantaneous shear modulus vary linearly, $\rho(x)/\rho(0) = G_0(x)/G_0(0) = 1 + (e^{-2} - 1)x$, over the same range as in the case of their exponential variation:

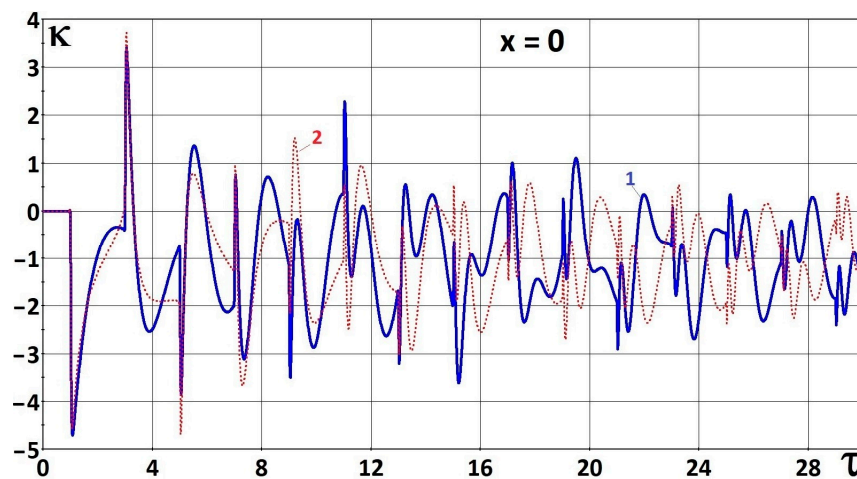


Figure 4. Relative stress–time history at $x = 0$ for the case of an exponential decrease in FGM properties with increasing x (curve 1) and linear decrease (curve 2).

Note that both for the first and the second fronts, which arrived to the fixed boundary from the loaded surface, the relative stresses with exponential and linear dependence of the material properties on the coordinate differ insignificantly.

In Figure 5, curve 1 corresponds to the input data with exponentially increasing density and shear modulus from the fixed boundary to the loaded surface:

$$\nu_0 \equiv 0.3, \rho(x)/\rho(0) = G_0(x)/G_0(0) = e^{2x}, \gamma_v \equiv 0, \gamma_s = \gamma_s(\tau) = 0.1e^{-0.3\tau}\tau^{-0.2}$$

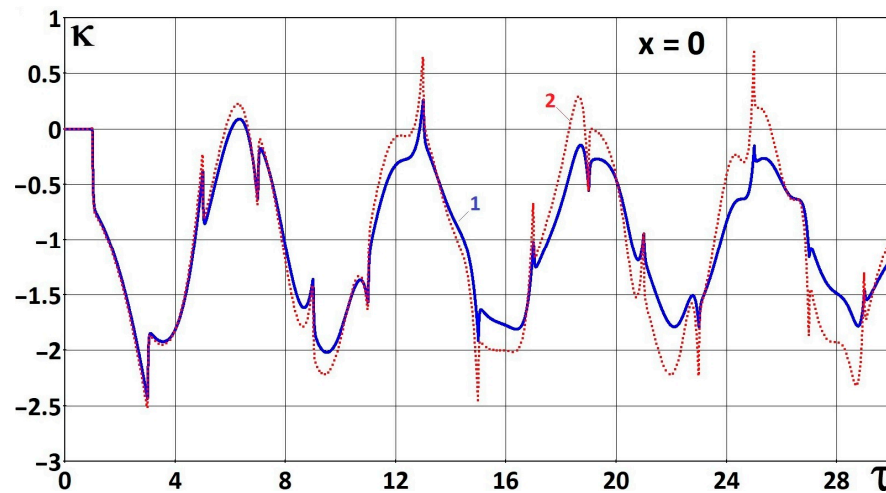


Figure 5. Time history of the relative stress at $x = 0$ for the case of an exponential increase in FGM properties with increasing x . Viscoelastic FGM—curve 1, elastic FGM—curve 2.

Curve 2 is obtained for $\gamma_v \equiv \gamma_s \equiv 0$ (linear elastic material).

It can be seen that with this type of inhomogeneity, the tensile stresses at the fixed boundary for the elastic material are far from being as large as those shown in Figure 3. For the viscoelastic material, they are not significant at all.

Figures 3–5 demonstrate the influence of the viscoelastic properties of the material on the wave process. It can be seen that the viscosity is practically not manifested for a relatively short time from the moment when the first disturbance front arrives from the boundary, where the load is applied, to the observation point. Further on, in contrast to the elastic FGM, in the viscoelastic FGM, the wave process gradually decays. Note that for the chosen external load, the relative stress $\kappa(x, \tau)$ tends to minus unity over time at all points of the layer. This follows from the analysis of the solution of the problem, and is also confirmed by the corresponding calculations.

Thus, the proposed approach, based on a hybrid numerical–analytical solution strategy, is suitable for applications over an arbitrary range of time intervals and does not require the viscosity to be small. This makes it possible for the first time to simulate a transient wave process in a viscoelastic FGM layer with a singular relaxation kernel.

5. Formulation of the Dynamics Problem for an Inhomogeneous Viscoelastic Cylinder

Let us consider the problem of non-stationary wave propagation in the cross section of a viscoelastic infinitely long hollow cylinder, whose material parameters depend continuously on the radial coordinate R (R, θ —polar coordinates in the cross-section plane, $R_0 \leq R \leq R_{\max}$). The cylinder is initially at rest, its outer surface $R = R_{\max}$ is free, and the inner surface ($R = R_0$), starting at time $t = 0$, is subject to a radial load $Q(t)$, which is constant along the generatrix of the cylinder. Thus, the wave process propagates in the direction of the variation of the material properties. The dimensionless quantities used to formulate the dynamic problem here are:

$$\begin{aligned}
 r &= R/R_{\max}, r_0 = R_0/R_{\max}, \tau = t/t_0, q_0 f(\tau) = Q(t)/[2G_0(r_0)], \\
 u(r, \tau) &= u_R(R, t)/R_{\max}, \sigma_r(r, \tau) = P_R(R, t)/[2G_0(r)], \\
 \sigma_\theta(r, \tau) &= P_\theta(R, t)/[2G_0(r)], \gamma_s(r, \tau) = t_0 T_s(R, t), \gamma_v(r, \tau) = t_0 T_v(R, t),
 \end{aligned}$$

where $t_0 = R_{\max}/c(1)$; $u_R(R, t)$, $P_R(R, t)$, $P_\theta(R, t)$ are the radial displacement, the radial and the circumferential stresses, respectively; q_0 is a dimensionless constant, $T_s(R, t)$, $T_v(R, t)$ are the viscoelastic kernels. The functions $c(r)$, $w(r)$, $G_0(r)$, $\nu_0(r)$, $\rho(r)$ have the same meaning as in the problem in the previous section. Figure 6a shows the loading conditions as a function of the dimensionless time.

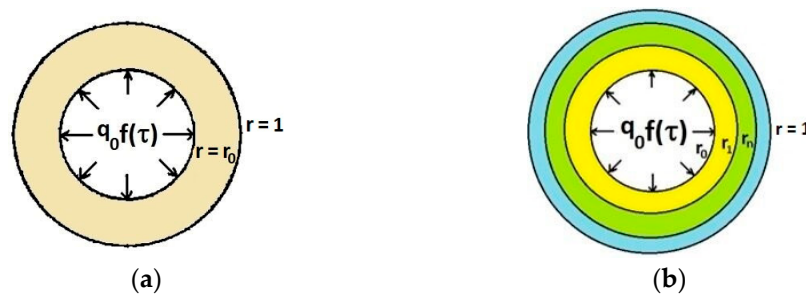


Figure 6. Loading conditions (a) cylinder of FGM; (b) piecewise homogeneous cylinder.

The mathematical formulation of the problem in the dimensionless form includes the dynamics equation in polar coordinates:

$$\frac{\partial \sigma_r(r, \tau)}{\partial r} + \left\{ \frac{d}{dr} \ln \left[\frac{G_0(r)}{G_0(r_0)} \right] \right\} \sigma_r(r, \tau) + \frac{\sigma_r(r, \tau) - \sigma_\theta(r, \tau)}{r} = w(r) \frac{c^2(1)}{c^2(r)} \frac{\partial^2 u(r, \tau)}{\partial \tau^2} \quad (14)$$

with boundary conditions:

$$\sigma_r(r_0, \tau) = -q_0 f(\tau), \sigma_r(1, \tau) = 0, \tau > 0 \quad (15)$$

initial conditions:

$$u(r, 0) = 0, \frac{\partial u}{\partial \tau}(r, 0) = 0 \quad (16)$$

where

$$\sigma_r(r, \tau) = w(r)(1 - \hat{d}_1) \frac{\partial u(r, \tau)}{\partial r} + (w(r) - 1)(1 - \hat{d}_2) \frac{u(r, \tau)}{r} \quad (17)$$

$$\sigma_\theta(r, \tau) = w(r)(1 - \hat{d}_1) \frac{u(r, \tau)}{r} + (w(r) - 1)(1 - \hat{d}_2) \frac{\partial u(r, \tau)}{\partial r} \quad (18)$$

$$\hat{d}_j \xi(\tau) = \int_0^\tau d_j(r, \tau - \chi) \xi(\chi) d\chi, j = 1, 2 \quad (19)$$

$$d_1(r, \tau) = \frac{1}{3 [1 - \nu_0(r)]} \{ [1 + \nu_0(r)] \gamma_v(r, \tau) + 2 [1 - 2\nu_0(r)] \gamma_s(r, \tau) \} \quad (20)$$

$$d_2(r, \tau) = \frac{1}{3\nu_0(r)} \{ [1 + \nu_0(r)] \gamma_v(r, \tau) - [1 - 2\nu_0(r)] \gamma_s(r, \tau) \} \quad (21)$$

Consider the problem with the same boundary conditions for a piecewise-homogeneous cylinder with the same inner and outer radii R_0 and R_{\max} , consisting of N homogeneous coaxial layers: $R_{n-1} \leq R \leq R_n, n = 1, 2, \dots, N; R_N = R_{\max}; N \gg 1$, with continuity conditions for the displacement and stresses vectors at the layer interfaces. For each n th layer, the displacement and stresses are designated by $u_R^{(n)}(R, t)$, $P_R^{(n)}(R, t)$, $P_\theta^{(n)}(R, t)$; the material parameters and functions $G_0^{(n)}, \nu_0^{(n)}, w_n, \rho_n, c_n, \alpha_n, T_v^{(n)}(t), T_s^{(n)}(t)$ have the same

meaning as in the problem for the piecewise-homogeneous layer. Using the piecewise-homogeneous hollow cylinder, we approximate the material properties of the functionally graded material using the relations ($n = 1, 2, \dots, N$):

$$G_0^{(n)} = G_0(r_n), \nu_0^{(n)} = \nu_0(r_n), \rho_n = \rho(r_n), \gamma_v^{(n)}(\tau) = \gamma_v(r_n, \tau), \gamma_s^{(n)}(\tau) = \gamma_s(r_n, \tau).$$

Here $r_n = R_n/R_N, \tau = t/t_0, t_0 = R_{\max}/c(1) = R_N/c_N$, as $c_n = c(r_n)$. Thus, $\gamma_v^{(n)}(\tau) = t_0 T_v^{(n)}(t), \gamma_s^{(n)}(\tau) = t_0 T_s^{(n)}(t), q_0 f(\tau) = Q(t)/(2G_0^{(1)})$. Let us introduce the dimensionless quantities $u^{(n)}(r, \tau) = u_R^{(n)}(R, t)/R_N, \sigma_r^{(n)}(r, \tau) = P_R^{(n)}(R, t)/(2G_0^{(n)}), \sigma_\theta^{(n)}(r, \tau) = P_\theta^{(n)}(R, t)/(2G_0^{(n)})$, where $r = R/R_N, r_0 = R_0/R_N$. The corresponding arrangement is depicted in Figure 6b).

The formulation of the problem for the layered cylinder consists of the dynamic equations:

$$(1 - \hat{d}_1^{(n)}) \frac{\partial}{\partial r} \left[\frac{\partial u^{(n)}(r, \tau)}{\partial r} + \frac{u^{(n)}(r, \tau)}{r} \right] - d_n^2 \frac{\partial^2 u^{(n)}(r, \tau)}{\partial \tau^2} = 0, \quad n = 1, 2, \dots, N \quad (22)$$

with the boundary conditions:

$$\sigma_r^{(1)}(r_0, \tau) = -q_0 f(\tau), \sigma_r^{(N)}(1, \tau) = 0, \tau > 0 \quad (23)$$

the conditions at the interfaces between the layers ($m = 1, 2, \dots, N - 1$):

$$u^{(m)}(r_m, \tau) = u^{(m+1)}(r_m, \tau), G_0^{(m)} \sigma_r^{(m)}(r_m, \tau) = G_0^{(m+1)} \sigma_r^{(m+1)}(r_m, \tau) \quad (24)$$

and the initial conditions:

$$u^{(n)}(r, 0) = 0, \frac{\partial u^{(n)}}{\partial \tau}(r, 0) = 0 \quad (25)$$

where

$$\sigma_r^{(n)}(r, \tau) = w_n (1 - \hat{d}_1^{(n)}) \frac{\partial u^{(n)}(r, \tau)}{\partial r} + (w_n - 1) (1 - \hat{d}_2^{(n)}) \frac{u^{(n)}(r, \tau)}{r} \quad (26)$$

$$\sigma_\theta^{(n)}(r, \tau) = w_n (1 - \hat{d}_1^{(n)}) \frac{u^{(n)}(r, \tau)}{r} + (w_n - 1) (1 - \hat{d}_2^{(n)}) \frac{\partial u^{(n)}(r, \tau)}{\partial r} \quad (27)$$

$$\hat{d}_j^{(n)} \xi(\tau) = \int_0^\tau d_j^{(n)}(\tau - \chi) \xi(\chi) d\chi, \quad j = 1, 2, \quad (28)$$

$$d_1^{(n)}(\tau) = \frac{1}{3(1 - \nu_0^{(n)})} [(1 + \nu_0^{(n)}) \gamma_v^{(n)}(\tau) + 2(1 - 2\nu_0^{(n)}) \gamma_s^{(n)}(\tau)] \quad (29)$$

$$d_2^{(n)}(\tau) = \frac{1}{3\nu_0^{(n)}} [(1 + \nu_0^{(n)}) \gamma_v^{(n)}(\tau) - (1 - 2\nu_0^{(n)}) \gamma_s^{(n)}(\tau)], \quad n = 1, 2, \dots, N \quad (30)$$

It is assumed that $\gamma_s^{(n)}, \gamma_v^{(n)}$ satisfy the conditions of limited creep.

The solution of the problem is constructed using the integral Laplace transform with respect to time, followed by inversion, just as it was performed for the case of the piecewise-homogeneous layer. A rather bulky solution of the problem in Equations (22)–(30) is presented in its most convenient form in [39]. In our case, the process of constructing originals for different types of relaxation kernels is similar to that described for the layer composed of the piecewise-homogeneous layers. We only note that for the regular kernels of the form (11), the solution in the originals for the displacement and stresses is obtained in the form of a series in residues similar to (12). For kernels of a more general form, formulas similar to (13) can be used.

6. Numerical Results for a FGM Viscoelastic Cylinder

Using the numerical implementation of the solution of the unsteady dynamic problem for a multilayer cylinder, the wave processes for a FG cylinder with different initial data can be investigated. In the approximation by the homogeneous layers of the continuously varied material properties and different types of inhomogeneity, the convergence of the results with an increase in the number of approximating layers under the condition $\lim_{\tau \rightarrow 0} f(\tau) = 0$ is verified. In particular, for the examples of continuous inhomogeneity given below, it turned out to be quite sufficient to limit the number of layers to 80 (as in the problem considered previously, the layers are equally thick). Note that when investigating the change in the nature of the wave process in the cylinder with increasing the number of sub-layers, the circumferential stress jumps $|\sigma_{\theta}^{(m)}(r_m, \tau) - \sigma_{\theta}^{(m+1)}(r_m, \tau)|$ at the contact between the adjacent layers tend uniformly to zero with respect to time.

As in the previous case of a layer composed of FGM, in the problem for an infinite hollow cylinder of FGM, along with the study of the convergence of the calculation process with increasing in the number of sublayers, the validity of the results is also confirmed by a verification study similar to that described in the previous Section 4. Additionally, for the particular case of $N = 1$ (homogeneous viscoelastic infinite hollow cylinder), the results obtained here using the integral Laplace transform and subsequent inversion were compared with the results obtained using finite element modeling in ABAQUS environment, and a very good agreement between these results was demonstrated in [41].

In the next figures, the results obtained for the case when $f(\tau) = (1 - e^{-50\tau})h(\tau)$, $r_0 = 0.5$ with the following FGM parameters:

$$\nu_0 \equiv 0.3; \rho(r)/\rho(r_0) = G_0(r)/G_0(r_0) = e^{3(r_0-r)}; \gamma_v(\tau) \equiv 0; \gamma_s = \gamma_s(\tau) = 0.2e^{-0.3\tau}\tau^{-0.4}.$$

Thus, only the density and the instantaneous shear modulus are dependent on the coordinate. They decrease exponentially starting from the loaded boundary to the free one. However, the velocity of longitudinal elastic waves does not depend on r . Note that in the studied case, the external load $Q(t)$ tends to $2G_0(r_0)q_0$ for $t \rightarrow \infty$. As mentioned previously, the negative stresses are compressive ($q_0 > 0$). All presented results for the FGM were obtained with $N = 80$.

In order to make a comparison, the selected characteristics of the wave process were also calculated for a cylinder consisting of only two homogeneous layers ($N = 2$) with the same $f(\tau)$ and r_0 , and the following input data:

$$r_1 = 0.75; \nu_0^{(1)} = \nu_0^{(2)} = 0.3; G_0^{(2)}/G_0^{(1)} = \rho_2/\rho_1 = e^{3(r_0-1)} = e^{-1.5};$$

$$\gamma_v^{(1)} \equiv \gamma_v^{(2)} \equiv 0; \gamma_s^{(1)} = \gamma_s^{(2)} = 0.2e^{-0.3\tau}\tau^{-0.4}.$$

The dynamic process characteristics in the two-layer cylinder with a discontinuous change in the properties of the material of the sub-layers at the boundary $r_1 = 0.75$ were compared to those in a FGM cylinder with a monotonic continuous change in the properties in the range from the largest value corresponding to the properties of the first layer of a two-layer cylinder to the smallest value corresponding to the properties of the second layer. Thus, the following equalities were satisfied:

$$G_0^{(2)}/G_0^{(1)} = \rho_2/\rho_1 = G_0(1)/G_0(r_0) = \rho(1)/\rho(r_0).$$

As is well known, one of the advantages of FGM compared to traditional layered homogeneous materials is the ability to avoid stress discontinuities in structural elements that can lead to delamination. In this regard, it is important to compare the dynamic processes in the FGM and the two-layer composite for some specific locations.

In Figure 7, curve 1 is the variation with the time of the relative circumferential stress κ_θ defined as

$$\kappa_\theta(r, \tau) = G_0(r)\sigma_\theta(r, \tau) / [G_0(r_0)q_0] = P_\theta(R_{\max}r, t_0\tau) / [2G_0(r_0)q_0]$$

at point $r = 0.75$ of the FGM cylinder. The same figure shows graphs of the variation with the time of the relative circumferential stress for the two-layer cylinder ($N = 2$):

$$\kappa_\theta^{(n)}(r, \tau) = G_0^{(n)}\sigma_\theta^{(n)}(r, \tau) / (G_0^{(1)}q_0) = P_\theta^{(n)}(R_Nr, t_0\tau) / (2G_0^{(1)}q_0), \quad n = 1, 2,$$

at the contact interface $r = 0.75$ in the first, stiffer layer ($n = 1$, curve 2a) and in the second ($n = 2$, curve 2b). Curve 3 shows the time variation of the relative stress $\kappa_\theta^{(1)}$ at point $r = 0.75$ for the homogeneous cylinder ($N = 1$) with the same $f(\tau)$, r_0 , $\nu_0^{(1)}$, $\gamma_v^{(1)}$, $\gamma_s^{(1)}$.

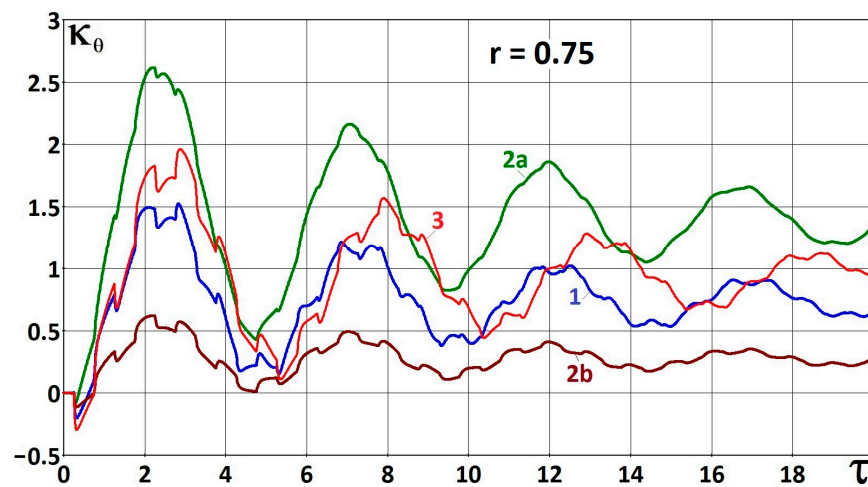


Figure 7. Time history of the relative circumferential stress at $r = 0.75$. Viscoelastic materials. FGM cylinder—curve 1; two-layer cylinder—curves 2a (inner layer) and 2b (outer layer); homogeneous cylinder—curve 3.

In Figure 8 are presented similar results for the case of the linear elastic materials (all relaxation kernels are zero). At the same time, all other input data for each of the curves are absolutely the same as for the corresponding curves in Figure 7.

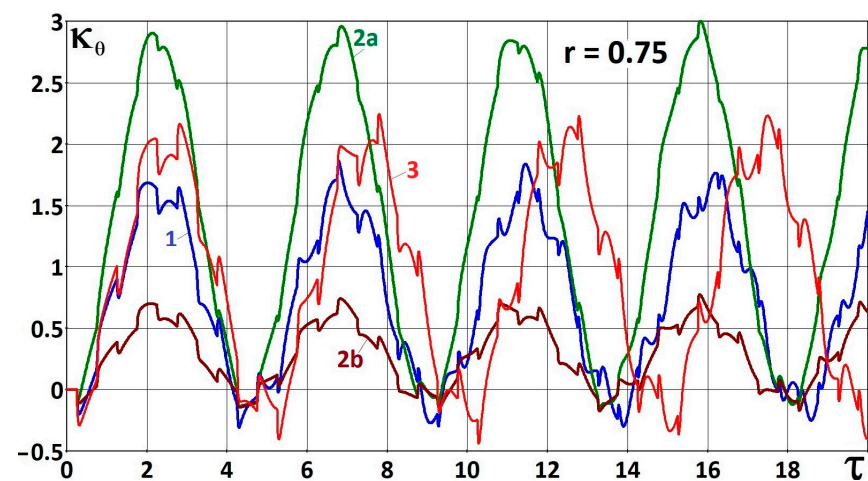


Figure 8. Time history of the relative circumferential stress at $r = 0.75$. Elastic materials. FGM cylinder—curve 1; two-layer cylinder—curves 2a (inner layer) and 2b (outer layer); homogeneous cylinder—curve 3.

Curves 2a and 2b in Figures 7 and 8 demonstrate a significant discontinuity in the circumferential stresses at the interface of the homogeneous components in the case of a two-layer material.

In all the subsequent figures, only three graphs are presented, since for the relative circumferential stress they correspond to the internal ($r = 0.75$), or external ($r = 1$) boundaries of the cylinder section. The relative radial stress is continuous at the interface between the layers ($r = 0.75$). In each of Figures 9–14, the curves 1, 2, 3 correspond to the results for the FGM, the two-layer composite and the homogeneous material, respectively. The variation in time of the relative circumferential stress at $r = 0.5$ in the case of the viscoelastic materials is shown in Figure 9, and in the case of the elastic materials in Figure 10. Similar curves at $r = 1$ are shown in Figure 11 (for the viscoelastic materials) and in Figure 12 (for the elastic materials).

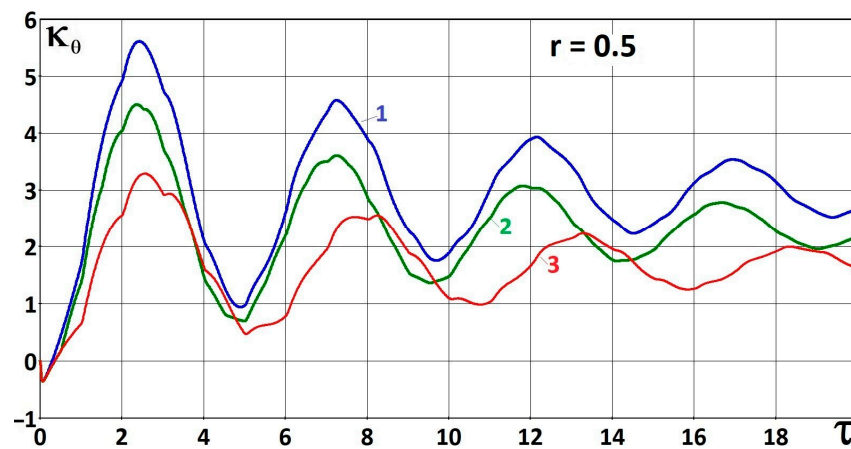


Figure 9. Time history of the relative circumferential stress at $r = 0.5$. Viscoelastic materials. FGM cylinder—curve 1; two-layer cylinder—curve 2; homogeneous cylinder—curve 3.

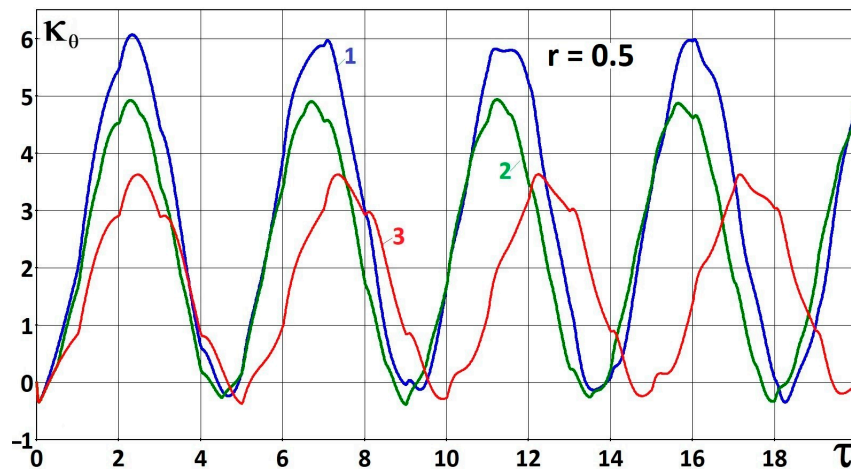


Figure 10. Time history of the relative circumferential stress at $r = 0.5$. Elastic materials. FGM cylinder—curve 1; two-layer cylinder—curve 2; homogeneous cylinder—curve 3.

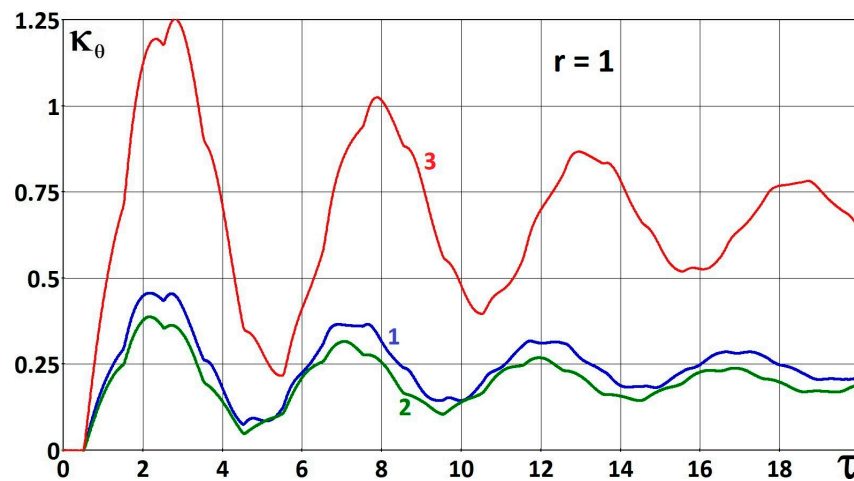


Figure 11. Time history of the relative circumferential stress at $r = 1$. Viscoelastic materials. FGM cylinder—curve 1; two-layer cylinder—curve 2; homogeneous cylinder—curve 3.

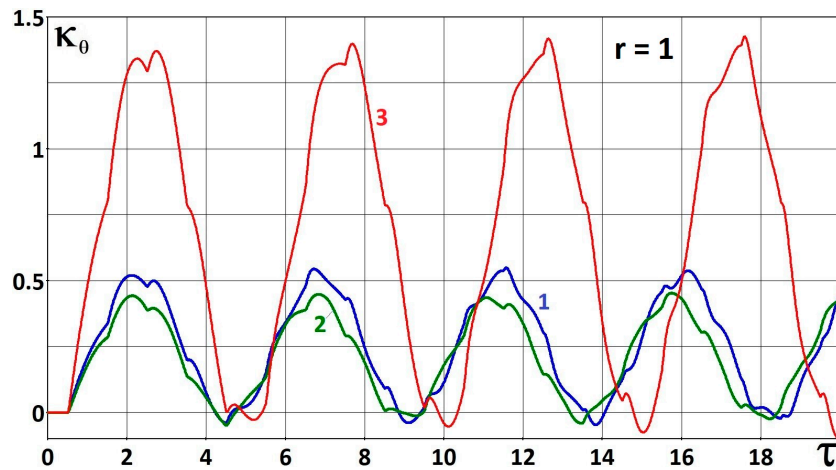


Figure 12. Time history of the relative circumferential stress at $r = 1$. Elastic materials. FGM cylinder—curve 1; two-layer cylinder—curve 2; homogeneous cylinder—curve 3.

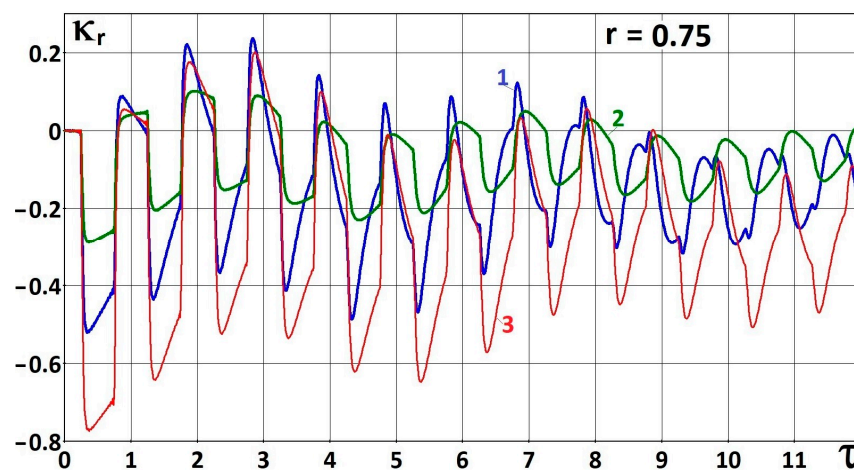


Figure 13. Time history of the relative radial stress at $r = 0.75$. Viscoelastic materials. FGM cylinder—curve 1; two-layer cylinder—curve 2; homogeneous cylinder—curve 3.

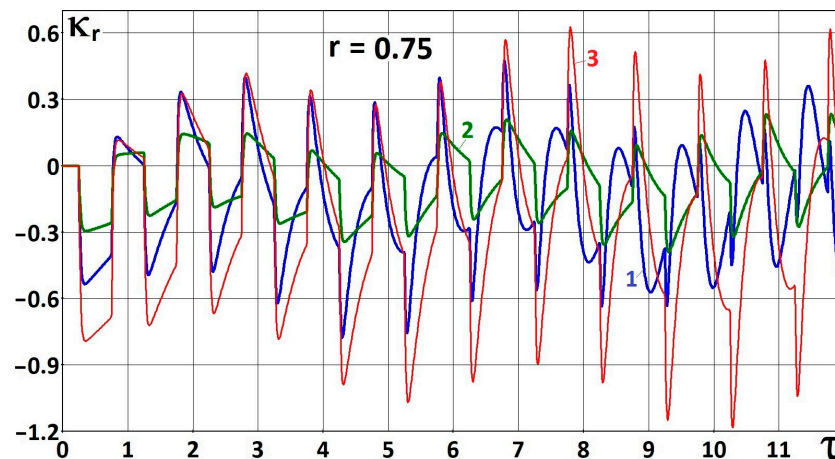


Figure 14. Time history of the relative radial stress at $r = 0.75$. Elastic materials. FGM cylinder—curve 1; two-layer cylinder—curve 2; homogeneous cylinder—curve 3.

Note that on the free boundary $r = 1$ the time histories of the circumferential stress in the case of the FGM and a two-layer material are very similar.

In Figures 13 and 14 are presented the time histories of the relative radial stress for the FGM,

$$\kappa_r(r, \tau) = G_0(r)\sigma_r(r, \tau) / [G_0(r_0)q_0] = P_R(R_{\max}r, t_0\tau) / [2G_0(r_0)q_0],$$

as well as for the two-layer composite ($N = 2$), and the homogeneous material ($N = 1$):

$$\kappa_r^{(n)}(r, \tau) = G_0^{(n)}\sigma_r^{(n)}(r, \tau) / (G_0^{(1)}q_0) = P_R^{(n)}(R_Nr, t_0\tau) / (2G_0^{(1)}q_0), \quad n = 1, N$$

at $r = 0.75$. Figure 13 is for the viscoelastic materials and Figure 14—for the elastic ones.

The presented results in Figures 9–14 demonstrate the influence on the considered nonstationary wave process of both the inhomogeneity of the material and its viscoelastic properties.

As for the case of a layer composed of FGM (Section 4), in the case of a hollow cylinder of the FGM, the viscosity practically does not have time to manifest itself within the relatively short times after the moment the first perturbation front arrives at the considered observation point. However, in contrast to the elastic FGM, in the viscoelastic FGM, the wave process gradually decays. For the external load, used in this study, the relative stresses $\kappa_r(r, \tau)$ and $\kappa_\theta(r, \tau)$ tend to the corresponding values in the solution of the static elastic problem, where the elastic characteristics of the FGM (approximated by the same systems of layers) are the long-term moduli corresponding to the considered relaxation kernels. This is confirmed by the calculations and agrees with the theoretical results in [38] related to the piecewise-homogeneous bodies. Thus, the proposed approach made it possible for the first time to model the transient wave process in a cylinder made of viscoelastic FGM with a singular relaxation kernel.

7. Conclusions

The results obtained show the possibility of using solutions of non-stationary dynamic problems for the corresponding piecewise-homogeneous (layered) solids in the problems of transient wave processes in functionally graded elastic and viscoelastic materials. We emphasize that here we focus on confirming the validity of applying the method of approximating the FGM by a layered structure, namely in nonstationary dynamic problems, despite the fact that the interfaces between the homogeneous layers are sources of additional perturbations. For the two problems considered here—an inhomogeneous infinite layer and an inhomogeneous infinite hollow cylinder—the convergence of the computed wave process characteristics to the dynamic FGM solution is confirmed as the number of layers used to approximate the varied material characteristics of the FGM increases.

To study wave processes in a layer of viscoelastic FGM, a solution to the problem of propagation of nonstationary waves in a piecewise-homogeneous linear viscoelastic layer (packet of homogeneous viscoelastic layers) is constructed. This solution is valid over the entire time range; it does not require the assumption of low viscosity and is convenient for numerical implementation. To study wave processes in a FGM hollow cylinder, we used the previously constructed solution of a non-stationary dynamic problem for a piecewise-homogeneous (multilayer) viscoelastic cylinder.

Based on the solutions of non-stationary dynamic problems for packages of parallel and coaxial cylindrical homogeneous viscoelastic layers, it is possible to study the transient wave processes in a layer and a hollow cylinder made of FGM and to demonstrate the influence of the viscosity and the inhomogeneity of the material on the dynamic response of such structures.

Author Contributions: Conceptualization, S.P. and M.D.; methodology, S.P.; writing—original draft preparation, S.P.; writing—review and editing, R.I. and M.D.; validation, R.I. and S.P. All authors have read and agreed to the published version of the manuscript.

Funding: This work was performed within the bilateral project funded by the Russian Foundation for Basic Research (project number 20-58-18002) and by the Bulgarian National Science Fund (project number KP-06-Russia/5 from 11.12.2020).

Conflicts of Interest: The authors declare no conflict of interest.

References

- De, S. Dynamic vibrations and stresses in a circular annulus of non-isotropic elastic material. *Pure Appl. Geophys.* **1972**, *93*, 68–72. [[CrossRef](#)]
- Senitskii, Y.É. Inhomogeneous anisotropic cylinder and sphere under an arbitrary radially symmetric dynamic load. *Sov. Appl. Mech.* **1978**, *14*, 451–456. [[CrossRef](#)]
- Saakyan, S.G. Waves in inhomogeneous elastic media. *Sov. Phys. Dokl.* **1986**, *31*, 852–853, translation from *Dokl. Akad. Nauk SSSR* **1986**, *290*, 1324–1327.
- Gubernatis, J.E.; Maradudin, A.A. A Laguerre series approach to the calculation of wave properties for surfaces of inhomogeneous elastic materials. *Wave Motion* **1987**, *9*, 111–121. [[CrossRef](#)]
- Ohyoshi, T. New stacking layer elements for analyses of reflection for transmission of elastic waves to inhomogeneous layers. *Mech. Res. Commun.* **1993**, *20*, 353–359. [[CrossRef](#)]
- Zhavoronok, S.I. Wave dispersion in heterogeneous waveguides: Methods of solution (a review). *Part 1. Mekhanika Kompoz. Mater. Konstr.* **2021**, *27*, 227–260. (In Russian) [[CrossRef](#)]
- Zhavoronok, S.I. Wave dispersion in heterogeneous waveguides: Methods of solution (a review). *Part 2. Mekhanika Kompoz. Mater. Konstr.* **2022**, *28*, 36–86. (In Russian) [[CrossRef](#)]
- Boggarapu, V.; Gujjala, R.; Ojha, S.; Acharya, S.; Venkateswara babu, P.; Chowdary, S.; Gara, D.K. State of the art in functionally graded materials. *Compos. Struct.* **2021**, *262*, 113596. [[CrossRef](#)]
- Swaminathan, K.; Naveenkumar, D.T.; Zenkour, A.M.; Carrera, E. Stress, free vibration and buckling analyses of FGM plates—a state-of-the-art review. *Compos. Struct.* **2015**, *120*, 10–31. [[CrossRef](#)]
- Punera, D.; Kant, T. A critical review of stress and vibration analysis of functionally graded shell structures. *Compos. Struct.* **2019**, *210*, 787–809. [[CrossRef](#)]
- Kuznetsov, S.V. Lamb waves in anisotropic functionally graded plates: A closed form dispersion solution. *J. Mech.* **2020**, *36*, 1–6. [[CrossRef](#)]
- Ilyashenko, A.; Kuznetsov, S. Dispersive waves in functionally graded plates. *MATEC Web Conf.* **2018**, *251*, 04052. [[CrossRef](#)]
- Bouhdima, M.S.; Zagrouba, M.; Ben Ghazlen, M.H. The power series technique and detection of zero-group velocity Lamb waves in a functionally graded material plate. *Can. J. Phys.* **2012**, *90*, 159–164. [[CrossRef](#)]
- Hu, Y.; Cao, X.S.; Niu, Y.; Ru, Y.; Shi, J. Asymptotic analytical solution on Lamb waves in functionally graded nano Copper layered wafer. *Appl. Sci.* **2021**, *11*, 4442. [[CrossRef](#)]
- Wang, X.; Li, F.; Zhang, X.; Yu, J.; Qiao, H. Thermoelastic guided wave in fractional order functionally graded plates: An analytical integration Legendre polynomial approach. *Compos. Struct.* **2021**, *256*, 112997. [[CrossRef](#)]
- Liu, C.; Yu, J.; Zhang, B.; Zhang, X.; Elmaimouni, L. Analysis of Lamb wave propagation in a functionally graded piezoelectric small-scale plate based on the modified couple stress theory. *Compos. Struct.* **2021**, *265*, 113733. [[CrossRef](#)]
- Han, X.; Liu, G.R.; Xi, Z.C.; Lam, K.Y. Characteristics of waves in a functionally graded cylinder. *Int. J. Numer. Methods Eng.* **2002**, *53*, 653–676. [[CrossRef](#)]

18. Egorova, O.V.; Kurbatov, A.S.; Rabinskiy, L.N.; Zhavoronok, S.I. Modeling of the dynamics of plane functionally graded waveguides based on the different formulations of the plate theory of I.N. Vekua type. *Mech. Adv. Mater. Struct.* **2021**, *28*, 506–515. [[CrossRef](#)]
19. Kielczynski, P.; Szalewski, M.; Balcerzak, A.; Wieja, K. Propagation of ultrasonic Love waves in nonhomogeneous elastic functionally graded materials. *Ultrasonics* **2016**, *65*, 220–227. [[CrossRef](#)]
20. Chen, W.Q.; Wang, H.M.; Bao, R.H. On calculating dispersion curves of waves in a functionally graded elastic plate. *Compos. Struct.* **2007**, *81*, 233–242. [[CrossRef](#)]
21. Ezzin, H.; Wang, B.; Qian, Z. Propagation behavior of ultrasonic Love waves in functionally graded piezoelectric-piezomagnetic materials with exponential variation. *Mech. Mater.* **2020**, *148*, 103492. [[CrossRef](#)]
22. Zhu, J.; Chen, W.Q.; Ye, G.R.; Fu, J.Z. Waves in fluid-filled functionally graded piezoelectric hollow cylinders: A restudy based on the reverberation-ray matrix formulation. *Wave Motion* **2013**, *50*, 415–427. [[CrossRef](#)]
23. Wang, Y.W.; Ren, H.Y.; Fu, T.R.; Shi, C.L. Hygrothermal mechanical behaviors of axially functionally graded microbeams using a refined first order shear deformation theory. *Acta Astronaut.* **2020**, *166*, 306–316. [[CrossRef](#)]
24. Saeed, I.T.; Chikh, A.; Tounsi, A.; Al-Osta, M.; Al-Dulaijan, S.U.; Al-Zahrani, M.M. Wave propagation analysis of a ceramic-metal functionally graded sandwich plate with different porosity distributions in a hygro-thermal environment. *Compos. Struct.* **2021**, *269*, 114030. [[CrossRef](#)]
25. Saeed, I.T.; Tounsi, A.; Chikh, A.; Al Osta, M.A.; Al-Dulaijan, S.U.; Al-Zahrani, M.M. An integral four-variable hyperbolic HSDT for the wave propagation investigation of a ceramic-metal FGM plate with various porosity distributions resting on a viscoelastic foundation. *Waves Random Complex Media* **2021**. [[CrossRef](#)]
26. Van Vinh, P.; Belarbi, M.-O.; Tounsi, A. Wave propagation analysis of functionally graded nanoplates using nonlocal higher-order shear deformation theory with spatial variation of the nonlocal parameters. *Waves Random Complex Media* **2022**. [[CrossRef](#)]
27. Tolokonnikov, L.A.; Larin, N.V. Scattering by a cylinder with an inhomogeneous coating of sound waves, emitted by a linear source in a plane waveguide. *Math. Model. Comput. Simul.* **2022**, *14*, 250–260. [[CrossRef](#)]
28. Larin, N.V.; Tolokonnikov, L.A. Sound scattering by a thermoelastic ball with a continuously inhomogeneous coating in a heat-conducting fluid. *Math. Model. Comput. Simul.* **2019**, *11*, 1007–1018. [[CrossRef](#)]
29. Han, X.; Liu, G.R.; Xi, Z.C.; Lam, K.Y. Transient waves in functionally graded cylinder. *Int. J. Solids Struct.* **2001**, *38*, 3021–3037. [[CrossRef](#)]
30. Medvedskiy, A.L. Problem of nonstationary elastic waves inhomogeneous transversely isotropic sphere diffraction. *Mekhanika Kompoz. Mater. Konstr.* **2008**, *14*, 473–489. (In Russian)
31. Zhou, L.; Ren, S.; Nie, B.; Guo, G.; Cui, X. Coupling Magneto-Electro-Elastic node-based smoothed radial point interpolation method for free vibration and transient analysis of Functionally Graded Magneto-Electro-Elastic structures. *Chin. J. Aeronaut.* **2020**, *33*, 227–243. [[CrossRef](#)]
32. Yu, J.G. Viscoelastic shear horizontal wave in graded and layered plates. *Int. J. Solids Struct.* **2011**, *48*, 2361–2372. [[CrossRef](#)]
33. Cao, X.; Jiang, H.; Ru, Y.; Shi, J. Asymptotic Solution and Numerical Simulation of Lamb Waves in Functionally Graded Viscoelastic Film. *Materials* **2019**, *12*, 268. [[CrossRef](#)]
34. Zhang, X.; Li, Z.; Wang, X.; Yu, J.G. The fractional Kelvin-Voigt model for circumferential guided waves in a viscoelastic FGM hollow cylinder. *Appl. Math. Model.* **2021**, *89*, 299–313. [[CrossRef](#)]
35. Vatulyan, A.O.; Varchenko, A.A. Investigation of Vibrations of a Beam Made of a Functionally Graded Material Taking into Account Attenuation. *Bull. High. Educ. Inst. N. Cauc. Region. Nat. Sci.* **2021**, *4*, 10–18. (In Russian) [[CrossRef](#)]
36. Korovaytseva, E.A.; Pshenichnov, S.G. The study of transient wave propagation in linearly viscoelastic bodies subject to the continuous heterogeneity of the material. *Probl. Prochnosti Plast.* **2016**, *78*, 262–270.
37. Bulychev, G.G.; Pshenichnov, S.G. Axisymmetric problem of long elastic inhomogeneous cylinder dynamics. *Stroit. Mekhanika Raschet Sooruzheniy* **1989**, *4*, 35–37.
38. Pshenichnov, S.G. Dynamic linear viscoelasticity problems for piecewise homogeneous bodies. *Mech. Solids* **2016**, *51*, 65–74. [[CrossRef](#)]
39. Pshenichnov, S.G.; Ryazantseva, M.Y.; Ivanov, R.; Datcheva, M.D. Dynamic problem for a viscoelastic hollow cylinder with coaxial elastic inclusion. *Comptes Rendus Acad. Bulg. Sci.* **2022**, *75*, 1184–1194. [[CrossRef](#)]
40. Ivanov, R.; Pshenichnov, S.G.; Datcheva, M.D. Non-stationary wave propagation in a viscoelastic layer due to step loading. In Proceedings of the iNDiS 2021, 15th International Scientific Conference, Novi Sad, Serbia, 24–26 November 2021; pp. 611–616.
41. Ivanov, R.I.; Pshenichnov, S.G.; Datcheva, M.D. Numerical validation of analytical solutions of non-stationary wave propagation problems. In Proceedings of the BGSIAM'21, 16th Annual Meeting of the Bulgarian Section of SIAM, Sofia, Bulgaria, 21–23 December 2021. [[CrossRef](#)]